# Using sub-micron silver-nanoparticle based films to counter biofilm formation by Gram-negative bacteria

Gillet, Alice; Baxter, Sean; Hodgson, Simon; Smith, G. C. ; Prabhakar, John Thomas

**Applied Surface Science**

*DOI:*
10.1016/j.apsusc.2018.02.116

Published: 01/06/2018

Peer reviewed version

# Using sub-micron silver-nanoparticle based films to counter biofilm formation by Gram-negative bacteria

A. R. Gillett[a,c], S. N. Baxter[b], S. D. Hodgson[a]*, G. C. Smith[c], P. J. Thomas[b]

[a]Department of Mechanical Engineering, Faculty of Science and Engineering, University of Chester, Chester, UK

[b]School of Chemistry, Bangor University, Bangor, UK

[c]Department of Natural Sciences, Faculty of Science and Engineering, University of Chester, Chester, UK

*corresponding author e-mail: s.hodgson@chester.ac.uk

## Abstract

Composite films comprised of silver nanoparticles (AgNPs) grown using a low-cost straightforward chemical bath based method have been deposited on glass microscope slides to investigate their potential as a sacrificial antibacterial coating. The as-deposited films have been characterised using scanning electron microscopy (SEM) and optical profilometry. These suggested that the films were relatively uniform in coverage. Chemical composition of the AgNP films has been studied by using x-ray photoelectron spectroscopy (XPS). The XPS analysis indicated that the Ag was in a metallic form able to sustain plasmon behaviour, and that low levels of residual nanoparticle precursors were present. Particle size was characterised using transmission electron microscopy (TEM) which showed an average particle size of 10.6 nm. The effectiveness of the films as an antibacterial coating was tested against *Escherichia coli*. The AgNP film was determined to be effective in the killing of *E.coli* cells over a 24 hour period when compared to equivalent samples that contained no silver. Of particular note was that only minimal bacterial growth was detected over the first 12 hours of testing, up to 78.6 times less than the control samples, suggesting the film is very efficient at slowing initial biofilm formation. The use of AgNP based films that have been synthesised using a novel low-cost, low-temperature and highly upscalable method is demonstrated as a promising solution for the deployment of silver as an effective sacrifical antimicrobial coating to counter the formation of potentially hazardous Gram negative biofilms.

Keywords: Silver nanoparticle, Antibacterial, XPS, TEM, biotechnology, E.coli.

## 1. Introduction

Silver nanoparticles (AgNPs) have been used for a wide range of applications in modern technology, due to their favourable chemical and physical characteristics. AgNPs can be synthesised by a variety of methods including laser ablation, flame pyrolysis, electrodeposition, microwave assisted, thermal evaporation & chemical vapour deposition, [1-6] . One key advantage of AgNPs is that they can be

easily synthesised by a variety of low in cost and highly scalable solution based methods [7-18]. AgNPs have been used in areas such as catalysis, plasmonic enhancement (e.g. of fluorescence or Raman scattering), as a way of enhancing drug potency, and as antifungal or antimicrobial compounds [19-23]. Due to their ease of synthesis they can be readily alloyed or functionalised (e.g. with gold) to further enhance or change aspects of their chemistry [24]. The use of these AgNPs as bactericides within the food and medical industries is of particular interest.

Bacteria are able to adapt to changing extracellular and environmental conditions. Because of this their ability to both adhere to, and form biofilms on, surfaces of many different types and structures is significant and makes them a potentially dangerous contaminant [25]. For example, within the food industry, food can be spoiled by the excessive build-up of bacteria on a surface. This sort of spoilage results in an increase in food wastage and increased cost to both manufacturers and inevitably, consumers. More dangerously, in medical technology, bacterial biofilms may cause infections which can lead to conditions ranging from mild short term illnesses to serious long term problems or even death. There have been many different methods employed in an effort to prevent the formation of biofilms on surfaces. These include surface modification (i.e. the generation of ordered surface structures by, for example, the use of laser processing), and surface coating [25, 26].

Despite the many positive factors associated with using AgNPs in human focused biological applications, there are still some negatives. Silver ions, of which nanoparticles within the body would become a source, are toxic to mammalian species in high levels. This phenomenon is well documented, with toxicity to multiple key organs having been observed although more evidence is needed to better understand the levels and mechanisms [27, 28]. A potential advantage of the using of nanoparticle based films for antibacterial applications is that they may provide a balance between acting as a source of sufficient silver to prevent unwanted biofilm formation whilst keeping the overall dose, and thus the toxicity, to a minimum. This could yield an ideal compromise between effectiveness and risk. Furthermore, the ability to control the total thickness of the nanoparticle film, by controlling growth rate and time, to as little as a single monolayer could lead to the design of sacrificial films that are able to dissipate after administering the necessary amount of silver. This paper explores the effectiveness of novel, low temperature, low cost, and easily scalable solution grown silver nanoparticle based films as an antibacterial coating against biofilm formation by gram-negative bacteria, namely *Escherichia coli*.

## 2. Experimental Techniques

### *2.1 Nanoparticle Synthesis and Film Deposition*

Synthesis of the Ag precursor, chlorotris(triphenylphosphine)silver(I) ($Ag(PPh_3)_3Cl$), was carried out using a modified method previously reported [29, 30]. All other chemicals were purchased from Sigma Aldrich and used without further purification. The Ag nanoparticle films were produced at the water-toluene interface using a method previously reported [31]. Briefly a toluene solution of $Ag(PPh_3)_3Cl$, (10 mL, 1.5 mM), was layered on top of aqueous sodium hydroxide (16 mL, 6.25 mM) in a clean 100 mL beaker. Identically sized beakers were used throughout to remove any effects caused by changing the diameter of the interface. The reactions were left to stand for, for approximately 10 minutes, to allow the phases to stabilise. To initiate the reaction, fresh aqueous tetrakishydroxymethylphosphonium chloride (THPC, 80% wt% in water) (330 µL, 50 mM) was injected down the walls of the beaker. The beaker was immediately transferred to a temperature

controlled oven at 50°C. Beakers were left for three hours, after which time a lustrous grey film was visible at the interface (Figure. 1). The final ligand is expected to be trihydroxy phosphine oxide (THPO) [32]. The as-grown films were subsequently transferred onto a glass substrate by piercing the film with a small piece of a standard sodium silicate glass microscope slide and then gently lifting the substrate at an angle through the film to deposit a thin layer of the nanoparticles onto the glass. The as-deposited films were left to dry in air overnight, prior to washing in fresh toluene and again being left to dry in air.

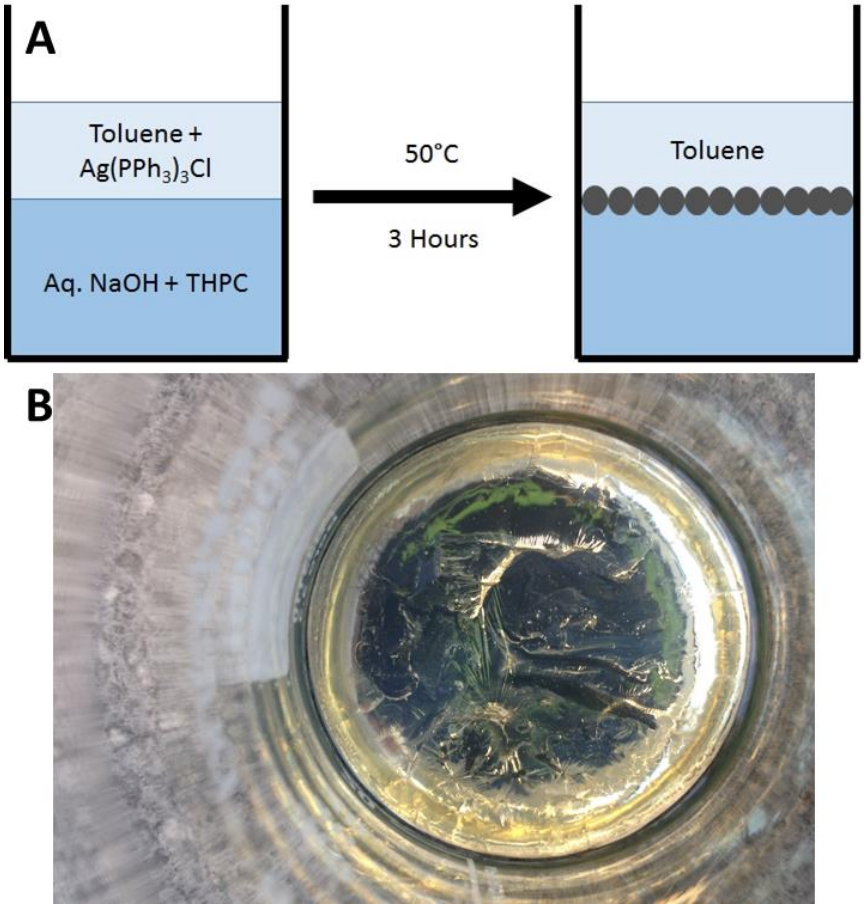


**Figure 1:** A) a simplified reaction scheme detailing the formation of a thin layer of Ag nanoparticles at the water-toluene interface. B) Top-down photograph of the as-formed film.

*2.2 Characterisation*

The surface topography of the AgNP films was characterised using a STIL Micromeasure 2 confocal chromatic imager. The scanning area was 25 × 25 µm, and the step size was approximately 75 nm. The Film thickness was approximated using both the Micromeasure 2 and a Taylor Hobson Form Talysurf Series 2 stylus profilometer. A Hitachi TM3030 benchtop scanning electron microscope (SEM) was used to take high resolution surface images. The surface chemistry of the silver nanoparticles was characterised using a custom ultra-high vacuum x-ray photoelectron spectroscopy

(XPS) system equipped with a 150 mm mean radius hemispherical energy analyser (Specs GmbH Phoibos 150) and a monochromatised Al Kα x-ray source at 1486.6 eV (Specs GmbH Focus 500). The scans were performed in medium area lens mode with a 7 mm diameter analyser aperture and a 30 mm lens iris. Survey scans were performed with a pass energy of 50 eV with scans over individual photoelectron lines performed at 15 eV. Samples were analysed as-received with no additional treatment. Data was quantified using Scofield cross sections corrected for the energy dependencies of the analyser transmission and the effective electron attenuation lengths. High resolution transmission electron microscope (TEM) images were acquired using a Philips CM20 TEM with particle size analysis performed manually with the assistance of ImageJ software. Samples were prepared for TEM analysis by sonicating an AgNP film in heptane to extract the particles, and pipetting a portion of the resulting mixture onto a holey carbon film TEM grid. This was allowed to dry in air leaving a small amount of the AgNPs on the grid ready for analysis. TEM images were taken at a range of magnifications with an accelerating voltage of 200 keV.

*2.3 Biofilm Formation and Image Analysis*

*Escherichia coli* (ATCC 25922), wild-type strain obtained from Oxoid Ltd was used as the model Gram negative bacteria. To assess the growth and viability of *E. coli* biofilms in the presence of AgNP films, AGNP samples were autoclaved at 121°C for 15 minutes, then aseptically placed in sterile petri dishes. Planktonic *E.coli* cultures were grown overnight in tryptone soya broth (TSB) under static growth conditions at 37°C. These overnight culture of *E. coli* were then diluted to an O.D. reading of 0.01 [33] before being added to the petri dishes. Samples were then incubated at 37$^{o}$C for prescribed time points, 6, 12 and 24 hours. The growth cycles of E.coli strains have been well characterised in the literature, and the time points have been chosen accordingly to approximately coincide with the growth, stationary and death phases [34-36]. After each time point, the samples were then aseptically removed and rinsed twice with sterile PBS to remove any planktonic bacteria before further analysis.

To prepare samples for SEM examination samples were washed with 0.1M sodium cacodyate and fixed with 2.5 % glutaraldehyde in 0.1M sodium cacodylate for 30 minutes. Fixed specimens were then washed twice in $dH_2O$ before being dehydrated for 10 minutes at each stage of an ascending methanol series (30 % to 100 %). They were then left to air dry for another 30 minutes. Each sample was coated in Au/Pd before SEM imaging.

Syto-9 and propodium iodide (PI) stains were used from a LIVE/DEAD BacLight Kit obtained from Thermofisher Scientific Inc. Syto-9 and PI were prepared according to the literature [37]. Working concentrations of 6.7 µM were prepared. Samples to be analysed were aseptically placed with the side to be analysed facing upwards in a clean sterile petri dish. While ensuring that exposure to light was minimal, the prepared working concentration of Syto-9 stain was carefully dispensed onto each sample. The plate was wrapped in aluminium foil, to protect form light exposure, and statically incubated at 30°C for 30 minutes. The stain was rinsed off using 0.9 % NaCl saline solution and samples were placed under a Leica DM2700 M fluorescence microscope for imaging. Area coverage and the ratio of live to dead cells were determined by post processing of the images with ImageJ software. Images were processed for red-blue-green colour with the green and red split channels selected. Particles of at least 6 pixels were analysed, excluding the edges and outlines, to determine the percentage area of the surface covered by bacterium [38].

## 3. Results and Discussion

### *3.1 Film Characterisation*

XPS spectra from the silver nanoparticle films are shown in Figure 2a with the elemental atomic percentage surface composition summarised in Table 1. As expected in a silver-based film, the dominant element found is silver. The binding energy of the Ag $3d_{5/2}$ peak was found to be 368.8 eV. This is ~0.5 eV higher than in the accepted reference value of 368.2 eV for bulk Ag [39] but the plasmon loss peaks visible at low level and approximately 4 eV displaced from their parent peaks in Figure 2b indicate the development of metallic structure and suggest the nanoparticles were sufficiently large, or the film structure suitable, to maintain a metal-like electronic structure typical of bulk Ag. Further, there is insufficient oxygen present for the shift to be accounted for by the presence of silver oxide. The small shift in binding energy of the Ag $3d_{5/2}$-$3d_{3/2}$ doublet relative to the reference value for metallic Ag is therefore attributed to charge transfer to the substrate. The O 1s peak (Figure 2c) was very broad and contained three sub peaks. The broad peak at the highest binding energy is an x-ray excited Na KLL Auger peak. The other two components, at binding energies of 531.2 and 532.7 eV are assigned to double bonded and single bonded oxygen respectively [40]. These assignments are consistent with the presence of the THPO ligand coordinated through the P=O group to the surfaces of the AgNPs, together with some intensity from the residual hydrocarbon species as seen in the carbon 1s peak (Figure 2d). The carbon peak shows a main component at 285.0 eV attributed to carbon in hydrocarbon bonds. Weak components are seen at higher binding energies corresponding to C-O (286.1 eV), C=O (287.5 eV) and COO- (288.9 eV) [40] functional groups and account for only 15 % of the total of approximately 27 at% of carbon. At these relatively low levels it is likely that these components are due to the general environmental contamination typically seen on samples exposed to the laboratory environment and as such can be discounted. Figure 2e shows the weak phosphorous 2p peak. The binding energy of ~133 eV is consistent with the 5-valent phosphorous of the THPO ligand [41]. The presence of Si is indicative of a small proportion of exposed substrate glass due to possible pinholes in the film. The low level of Na is also due to the underlying sodium silicate glass. Inspection of the survey spectrum showed that the low level of S detected was present with S 2p components at 161.6 eV and 168.7 eV in approximately equal proportions. These binding energies match well to reference data for sulphide and sulphate forms respectively [41]. Ag surfaces are known to be highly reactive to environmental sulphur, and the presence of sulphur is attributed to a low level of contamination of the original Ag source material. The presence of sulphate groups indicates oxidation of a proportion of this S during preparation. The presence of a low level of Cl suggests some unreduced THPC from the nanoparticle film formation reaction.

| Element & photoelectron line | Composition, atom % |
|---|---|
| **Ag 3d** | 52.3 |
| **O 1s** | 12.9 |
| **C 1s** | 27.4 |
| **Cl 2p** | 2.8 |

| | |
|---|---|
| **P 2p** | 2.5 |
| **S 2p** | 1.1 |
| **Si 2s** | 0.4 |
| **Na 1s** | 0.7 |

**Table 1:** XPS surface composition results from the Ag nanoparticle film

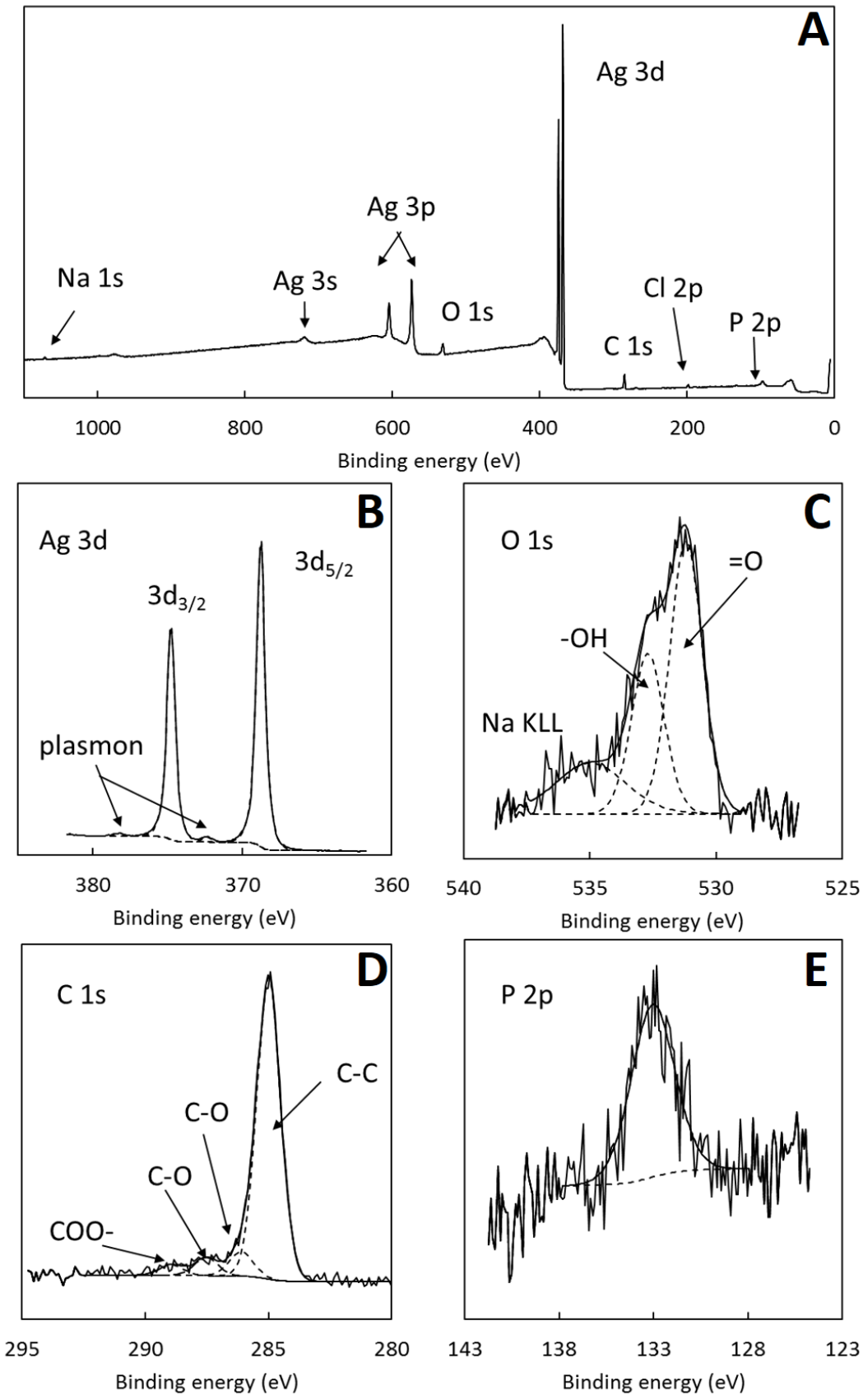


**Figure 2:** XPS spectra obtained from the Ag nanoparticle films showing the survey scan (upper panel) and high resolution scans over the Ag 3d, O 1s, C 1s and P 2p lines.

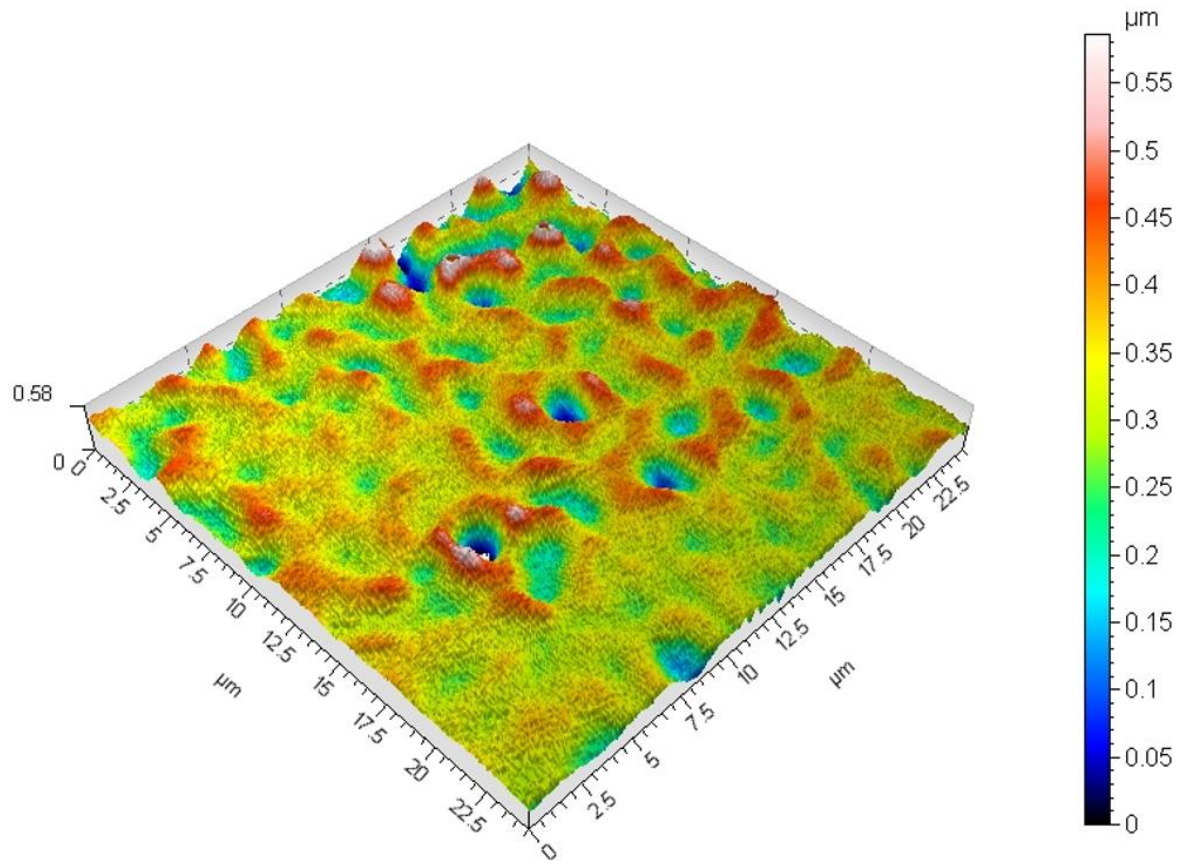


**Figure 3:** Surface profile of an Ag nanoparticle film.

A 3D surface map of the AgNP films is displayed in Figure 3. The mean surface roughness ($S_a$) was found to be 7.36 nm suggesting a comparatively uniform film. The kurtosis (Sku) value of 4.01 indicates the presence of some high peaks or valleys. These could simply be the pinhole defects described in the XPS. The comparatively low level of Kurtosis also suggests that the film is comparatively uniform. The uncoated substrate had a mean roughness of 76.1 nm and a kurtosis value of 3.36 demonstrating a smoothing effect caused by the AgNPs effectively filling in the gaps on the rougher glass substrate whilst also indicating a small increase in the amount of comparatively high peaks/valleys (due to a mixture of pinholes and aggregated particles). Film thickness measurements of the AgNP films are challenging. The difference in the reflectivity between the AgNP films and the substrate hinders the effectiveness of optically measuring the step height, and measurement using more physical means (such as stylus profilometry) also presents a problem due to the softness of the film. The softness can lead to film damage during measurement, caused by the styles tip, which results in unrealistic values. Using a combination of both of these techniques it has been possible to approximate the average thickness of these AgNP films as being of the order of ~500 nm. This is also supported by the surface shown in figure 3. Here the lowest pit, presumably a pinhole-type defect through to the glass substrate (as seen in the XPS), is ~550-600 nm below the highest points which are ~100-150 nm above the typical film surface height. Because of the easily

controllable methodology used to produce these AgNP films, through knowledge of the growth rate and careful manipulation of the precursor conditions, films as thin as a few atomic layers (< 50 nm) could be produced.

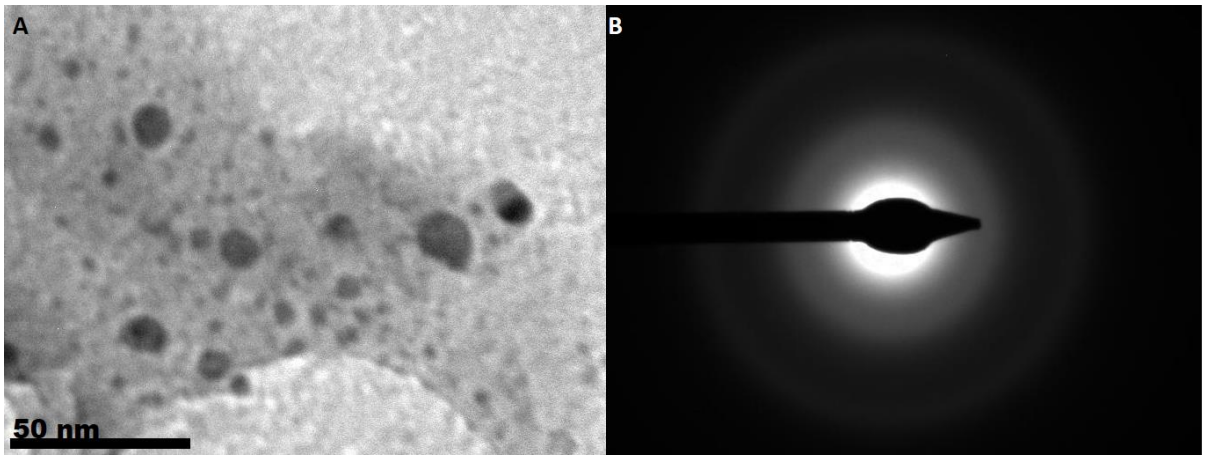


**Figure 4:** a) Transmission electron micrograph (TEM) showing several AgNPs, b) Selected area diffraction pattern of a typical AgNP showing evidence of polycrystallinity.

Figure 4a shows a TEM micrograph of several sonicated AgNPs. Particle size analysis of multiple micrographs provided an average nanocrystal diameter of 10.6 nm ±6.83. The high standard deviation is an indication of the variety of different nanoparticle sizes, with a small number of large, aggregated nanoparticles (the largest seen in an image being 52 nm) and some somewhat smaller AgNPs of the order of ~5 nm.

It should also be noted that due to their high surface energy relative to their size, the silver nanoparticles, as suggested in the XPS, may have agglomerated somewhat in the film (indeed Figure 5 also appears to show some patches of thicker silver where agglomeration has definitively taken place)[42]. The sample preparation for TEM was likely to have caused a level of deagglomeration to occur, as a result of sonication in the sample preparation. The nanoparticle sizes observed will therefore be a lower limit for the sizes of the particle agglomerations within the film that perform the bioactive role. Whilst the behaviour of agglomerations and individual nanoparticles will inevitably be different, the low level of preparation required to deagglomerate the sample for TEM measurement suggests that the individual nanoparticle portions may not be overly strongly bound to the agglomerate allowing them to detach easily.

Figure 4b displays a selected area diffraction pattern of a re-deposited AgNP film showing concentric rings indicating polycrystallinity [43] but without the individual diffraction spots seen in SAED patterns of highly crystalline Ag nanoparticles [44, 45].

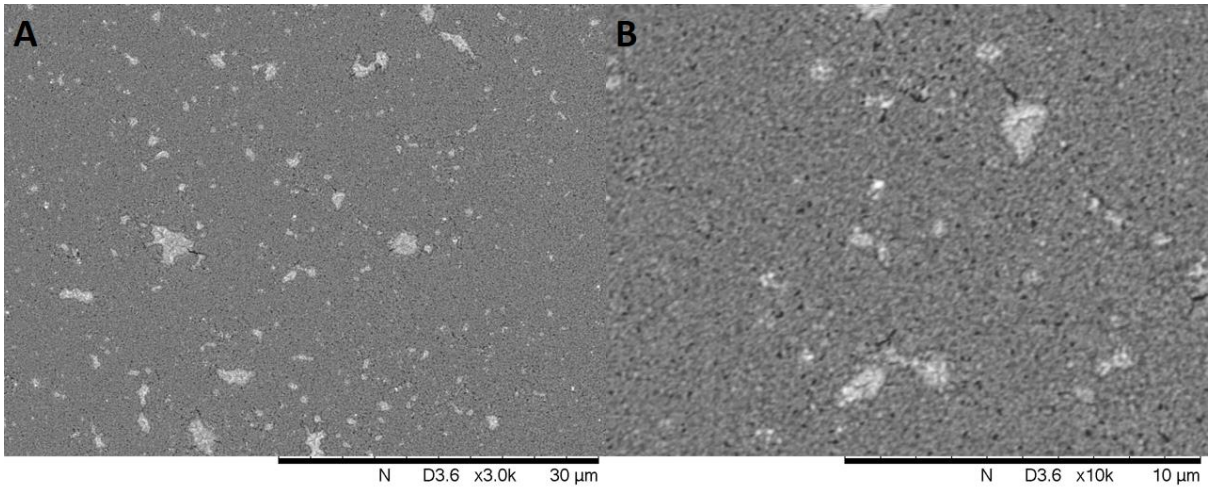


**Figure 5:** Scanning electron microscopy (SEM) of the AgNP films at a) 3,000× and b) 10,000× magnification.

SEM images of the as-deposited AgNP films are displayed in Figure 5. The film demonstrates a good level of coverage over the glass substrate, however there is also evidence of aggregation into clearly visible clumps, or thicker areas, of silver. As shown in Figure 6, these aggregates were not present on the surface of the samples that had been submerged in the TSB medium. This is indicative of a level of film degradation, which supports the idea of using these films as sacrificial layers. A sacrificial silver film would be capable of releasing a small amount of antibacterial silver particles before disappearing, although it should be stated that these sort of films would need to be thinner than those used in this study.

*3.2 Antimicrobial activity against E.coli*

Although the precise mechanisms of AgNP toxicity against Gram-negative bacteria are not fully understood [46], mechanisms and order of action of AgNPs have been proposed according to the morphological and structural changes caused to the bacterial cells [47]. Initial antibacterial action of AgNPs occurs through the release of silver ions ($Ag^+$) as well as from either disruption of or damage to the cell wall and membrane caused by the AgNPs themselves [46]. The nanoparticles are able to attach to the cell membrane and penetrate inside the bacteria, where the $Ag^+$ ions released may be lethal as they disrupt DNA replication, metabolism, cell signalling and cell division [46, 47]. SEM micrographs of *E.coli* adhered to surfaces with and without AgNP coating are displayed in Figure 6. Figure 6a shows the silver film after incubation in TSB as a control sample with no bacteria present. The silver shows, as would be expected, no growth of bacterial colonies. This demonstrates an absence of surface or broth contamination. Figures 6b and 6c display a control sample of the bare glass slide in the bacteria containing TSB. The *E. coli* cells, unexposed to silver, are smooth and show the typical characteristics of rod cell shape and size (~3 µm). The adhered cells exposed to the AgNP films, however, were damaged severely (Figures 6d-g). Many of the cells were noticeably translucent, suggesting leakage of internal cell content, and others were misshapen, with pits, and fragmented. With the cells that have flattened and taken on a translucent appearance it is possible to see the silver film through the cell in the images. This apparent transparency to the electrons of

the SEM suggests severe thinning of the bacterial cell structure, allowing contrast from the underlying substrate to be visible. Pit formation on the surface of *E.coli* cells post exposure to AgNPs has been frequently reported in the literature. Sondi and Salopek-Sondi, for example, demonstrated in their work the formation of pits within the cell membrane [48].

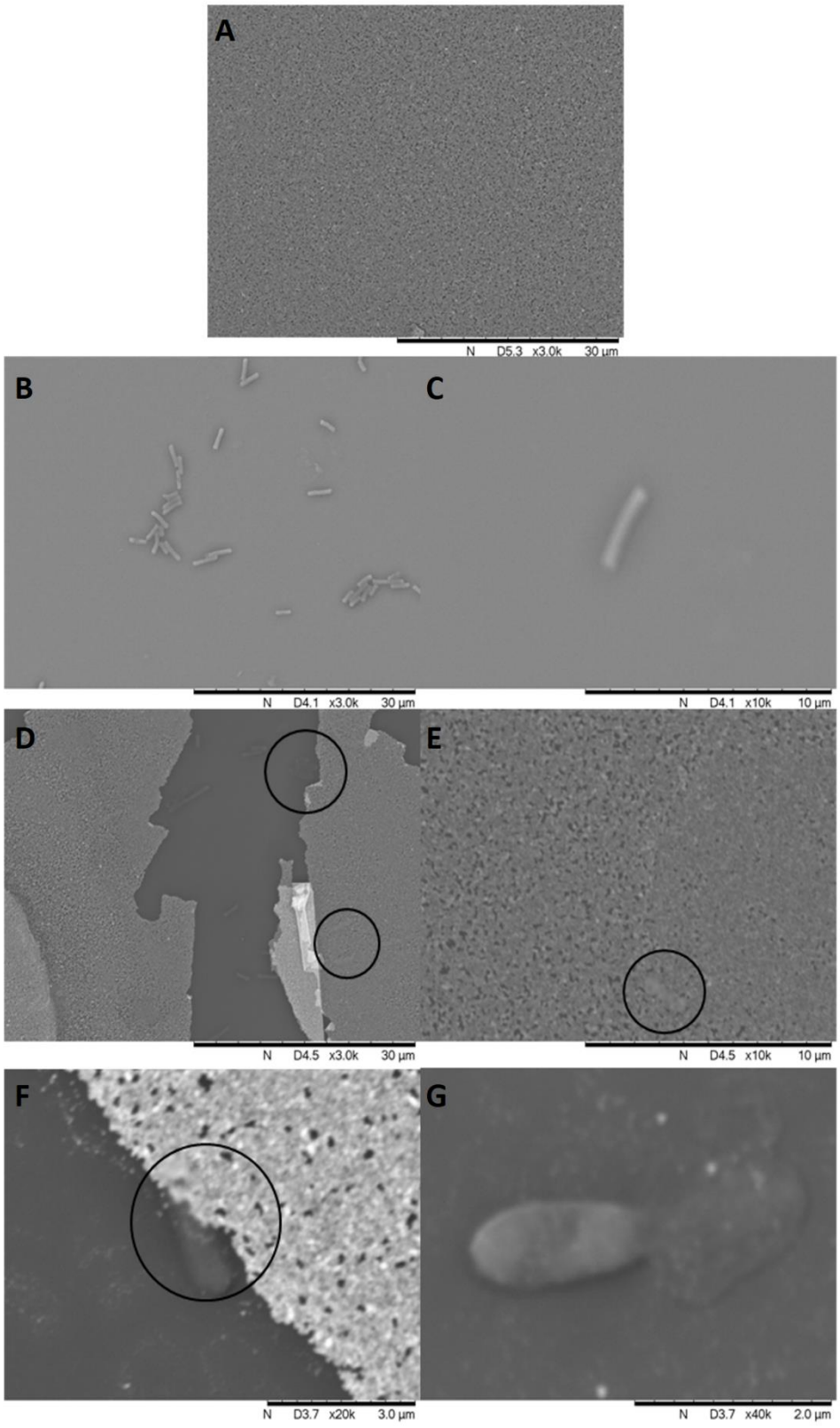


**Figure 6:** Scanning electron microscopy (SEM) of the AgNP films. A) Control sample of silver in TSB with no bacteria, B and C) *E.coli* adhered to glass reference sample after 24 hours of incubation in

TSB D-G) *E.coli* adhered to AgNP film samples after 24 hours of incubation in TSB. Denatured *E.coli* on (circled) Ag nanoparticle films after 24 hours of incubation.

Bactericidal effects of AgNP films were investigated against *E.coli* bacteria over a period of 24 hours, as demonstrated in Figure 7, by epifluorescence microscopy following Syto-9 and PI staining. The bacterial membrane permeability to these dyes depends upon the cell membrane integrity, therefore distinguishing the viability of the bacterial cell. Syto-9 is a small molecule capable of penetrating cell walls with relative ease, and stains the cells green, regardless of their viability. PI on the other hand cannot pass through intact cell membranes, so that only cells with compromised membranes can be labelled with this red fluorescent dye. From this, it is possible to infer that live bacteria will fluoresce green due to the presence of Syto-9, and the dead cells (i.e. those with compromised membranes) will fluoresce red due to the PI [49]. As demonstrated in Figure 6, the unexposed bacterial cells remain intact (i.e. green), whereas the *E.coli* exposed to the AgNP films are predominantly denatured (i.e. red). Therefore it can be inferred that the surface AgNPs exhibited a strong antibacterial effect at all the prescribed time points relative to the control samples. As the cells continued to grow over the investigated time period this supports, with the observations from the SEM images, that the E.coli cell membrane has been disaggregated supporting the cell membrane disruption mechanism of AgNPs. The images also show multiple comparatively dark areas with little/no coverage of bacteria. This could be indicative of morphological effects from the substrate (either coated or non-coated) influencing the location of initial bacterial attachment or providing areas for preferential growth. The greater average roughness measured on the glass substrate is highly likely to cause a more uneven distribution as, whilst it has been demonstrated that ordered micro/nanostructuring may inhibit bacterial attachment, features can provide preferential regions for bacteria to align with [25, 50].

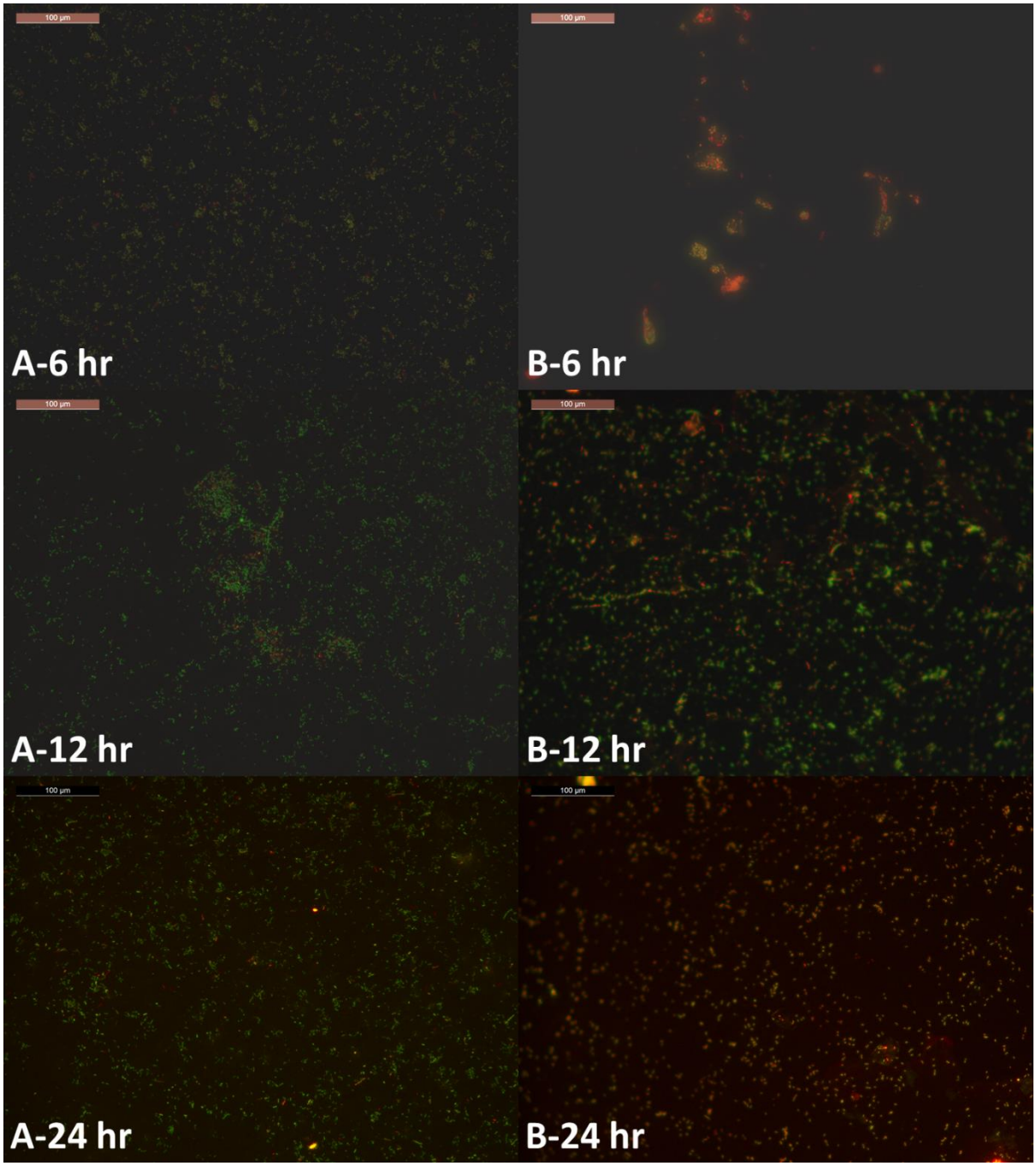


**Figure 7:** Fluorescence micrographs of A) the AgNP free control sample and B) the AgNP films after 6, 12 and 24 hours incubation time in TSB. The scale bar in the top left of each image is 100 µm. Green fluorescent colour indicates intact and live cells, whereas red fluorescent colour indicates dead cells with compromised cell membranes. It should be noted that whilst some of the images (e.g. B-12 hr) appear green to the eye, closer examination shows the interior of the bacteria stained red indicating cell death and the green appearance only showing from the outer cell membrane area.

*3.3 Percentage area coverage of viable E. coli cells*

Figure 8 displays the percentage area coverage results for both live and dead *E. coli* cells. It is readily observable that the AgNP film was highly effective at reducing the number of live E. coli cells adhered to the surface at all measured time periods (6, 12 and 24 hours). The glass control samples demonstrated an increase in the quantity of viable bacterial cells over the first 12 hours. In comparison, the AgNP coated samples showed a fairly constant level of viable cells with the quantity of dead cells increasing greatly. This confirms the bactericidal effect of the films. Crucially, the quantity of live bacterial cells seen on the surface of the AgNP coated slides is only minimal, relative to the control samples, after 6 hours suggesting that the AgNPs are very effective at slowing the initial formation of a live biofilm. The mean percentage area coverage for the control samples after 6 hours was found to be 2.38 ±0.80%, whereas the AgNP coated slides had a mean percentage coverage of 0.035 ±0.01%. This is 1.47 % of the coverage seen in the control sample, or a factor of 68.0 times less. After 12 hours the mean percentage area coverage for the control samples was found to be 5.50 ±1.17%, whereas for the AgNP coated samples the coverage was 0.07 ±0.05%. This equates to 1.27 % of the coverage seen in the control sample, or a factor of 78.6 times less coverage by live bacteria.

In comparison, the proportion of dead cells on the glass control slides stays comparatively constant over the 24 hours with the number of viable cells remaining constant, within error, between 12 and 24 hours. Alternatively the Ag films, after 24 hours, show an increase in the proportion of viable cells and a decrease in the proportion of dead cells in comparison to the films after 12 hours. After 24 hours, although the coverage of live cells has increased for the AgNP coated samples (1.92 ±0.71%), the area coverage is still only 42.29 % (a factor of 2.4 times less) of that observed on the control samples (4.54 ±1.52%). This could be due to either depletion of the film, reducing the bactericidal effect, or sufficient bacterial death as to provide a sort of barrier layer sufficient to limit the effects of silver on new bacteria, thus allowing them to begin to form a fresh biofilm. Whilst this leads to questions over the longevity of an AgNP film it would support the idea of the usage of the films as a sacrificial layer to prevent initial biofilm formation as there is a clear delay in significant bacterial growth. Indeed it was also noted that upon submersion into the TSB that the wash resistance of the silver film was limited, possibly indicating that this mechanism, i.e. film depletion, may be the primary reason for the improved bacterial growth with the AgNP films after 24 hours. Further improvements for the wash resistance and longevity of the coating may be required to optimise the layers. Polymer-coated silver nanoparticles have been shown to be more stable in both water and simulated biological fluids [51, 52]. It has also been found that AgNPs on bulk matrixes have weak washing resistance, however samples with a high wt% were still found to exhibit strong antimicrobial action after 120 hour wash test [53]. Therefore by improving the wash resistance of the AgNP film by immobilising them within the pores of porous substrates such as silica, long term antimicrobial activity with lower AgNP concentration may be achieved [54]. The standard deviations as a proportion of the bacterial coverage of both sets of samples are very similar. In the case of the silver coated samples, the proportional standard deviation is lower for the amount of dead bacteria (compared to the control) and larger for the live. This can be explained by the dominant effect of silver being to kill the bacteria. With relatively large numbers of dead bacteria on the surface the coverage will be more consistent from sample to sample, the reverse being true for the glass where, due to no additional threat to the bacteria's survival the live coverage is more consistent. Many factors will influence the regions of a substrate that bacteria adhere to, from composition, surface free energy, topography and micro-/nanoroughness. It is possible that the more-uneven surface of

the glass (as demonstrated in section 3.1) promotes a more uneven distribution of initial bacterial attachment.

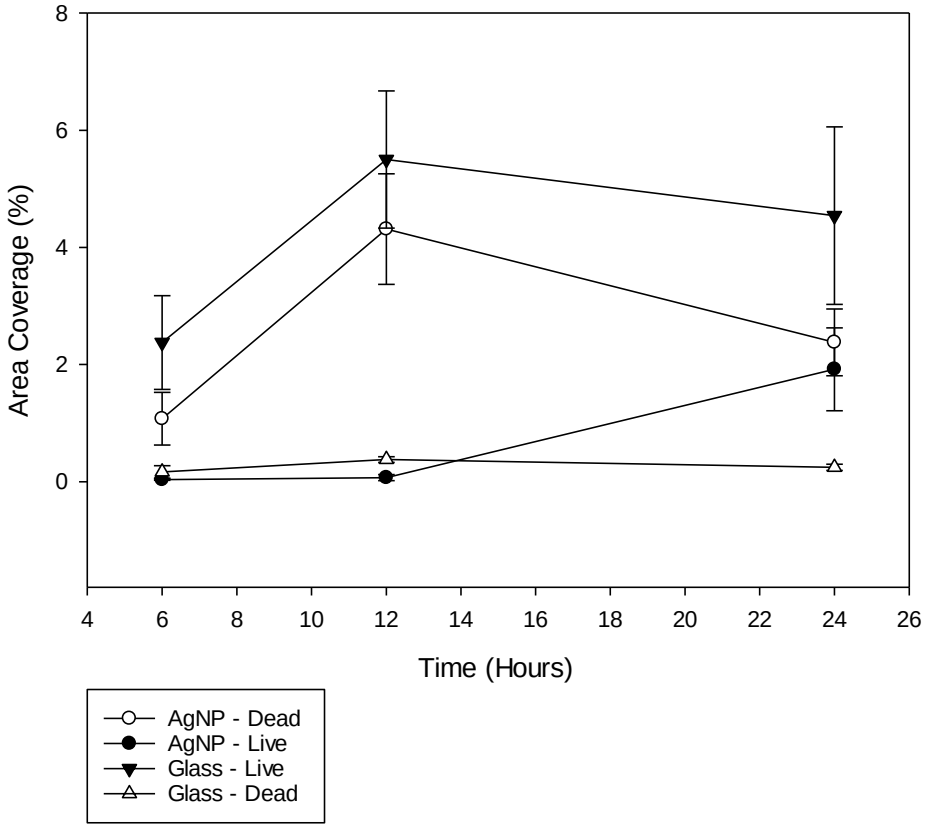


**Figure 8:** Mean percentage area covered by adhered *E. coli*, comparing the viability on the control and AgNP coated samples.

## 4. Conclusions

The antibacterial effect of AgNP films on Gram-negative *E. coli* bacteria has been explored as a method to limit biofilm formation. The films were deposited using a very simple, and highly controllable, low-cost one-pot synthesis. The films were approximately 500 nm in thickness and uniform in coverage. Chemical analysis suggested that a level of aggregation had occurred between the nanoparticles, with the TEM providing a lower size limit through particle size analysis which showed the average particle size to be ~10.6 nm in diameter. The TEM only provides a lower limit for the particle size as an aspect of the sample preparation results in a level of deagglomeration of the film. The AgNP films deposited on the glass slide have been shown to effectively kill *E.coli* bacteria in comparison to an uncoated slide. Samples exhibited higher percentage of dead cell adhered to the samples coated in the Ag film compared to that of the uncoated sample. With particular effectiveness within the first 12 hours when the levels of live bacteria detected on the surface was

up to 78.6 times lower than that observed on glass control samples. This demonstrates that the AgNPs are particularly effective at preventing initial biofilm formation, although the level of live bacteria does start to increase by 24 hours exposure time. With regards to the mechanism of antibacterial activity, the SEM images suggest a high degree of cell disruption. The SEM images display a severe loss of morphological integrity where the *E.coli* show differential structural loss in the flattening of the cell. This study suggests that the development of a very thin sacrificial antibacterial coating, for usage in the medical industry in particular, made up of AgNP based films is viable.

**Acknowledgements**

The authors from the University of Chester would like to acknowledge members of Miss Gillett's original supervisory team, Dr. Waugh and Prof. Lawrence, as well as helpful discussions from other members of the Department of Mechanical Engineering and the Department of Natural Sciences in the Faculty of Science and Engineering.

**References**

[1] M. Boutinguiza, R. Comesaña, F. Lusquiños, A. Riveiro, J. del Val, and J. Pou, "Production of silver nanoparticles by laser ablation in open air," *Applied Surface Science,* vol. 336, pp. 108-111, 2015.

[2] M. A. Valverde-Alva *et al.*, "Synthesis of silver nanoparticles by laser ablation in ethanol: A pulsed photoacoustic study," *Applied Surface Science,* vol. 355, pp. 341-349, 2015.

[3] K. J. Brobbey *et al.*, "One-step flame synthesis of silver nanoparticles for roll-to-roll production of antibacterial paper," *Applied Surface Science,* vol. 420, pp. 558-565, 2017.

[4] D. Zhang, Y. Tang, F. Jiang, Z. Han, and J. Chen, "Electrodeposition of silver nanoparticle arrays on transparent conductive oxides," *Applied Surface Science,* vol. 369, pp. 178-182, 2016.

[5] L. Peng, R. Guo, J. Lan, S. Jiang, and S. Lin, "Microwave-assisted deposition of silver nanoparticles on bamboo pulp fabric through dopamine functionalization," *Applied Surface Science,* vol. 386, pp. 151-159, 2016.

[6] X. Zhang *et al.*, "Growth graphene on silver–copper nanoparticles by chemical vapor deposition for high-performance surface-enhanced Raman scattering," *Applied Surface Science,* vol. 353, pp. 63-70, 2015.

[7] S. Y. Gao, D. Q. Yuan, J. Lu, and R. Cao, "In situ synthesis of Ag nanoparticles in aminocalix 4 arene multilayers," *Journal of Colloid and Interface Science,* vol. 341, no. 2, pp. 320-325, 2010.

[8] H. H. Park, X. Zhang, Y. J. Choi, H. Kim, and R. H. Hill, "Facile synthesis and size control of Ag nanoparticles by a photochemical reduction at room temperature," *Journal of the Ceramic Society of Japan,* vol. 118, no. 1383, pp. 1002-1005, 2010.

[9] H. B. Wang, Y. Y. Lou, and D. O. Northwood, "Synthesis of Ag nanoparticles by hydrolysis of Mg-Ag intermetallic compounds," *Journal of Materials Processing Technology,* vol. 204, no. 1-3, pp. 327-330, 2008.

[10] S. D. Oh *et al.*, "Synthesis of Ag and Ag-SiO2 nanoparticles by gamma-irradiation and their antibacterial and antifungal efficiency against Salmonella enterica serovar Typhimurium and

Botrytis cinerea," *Colloids and Surfaces a-Physicochemical and Engineering Aspects,* vol. 275, no. 1-3, pp. 228-233, 2006.
[11] D. H. Chen and Y. W. Huang, "Spontaneous formation of Ag nanoparticles in dimethylacetamide solution of poly(ethylene glycol)," *Journal of Colloid and Interface Science,* vol. 255, no. 2, pp. 299-302, 2002.
[12] H. A. Chaghouri, M. A. Malik, P. John Thomas, and P. Brien, "Assembly of Submicron Sized Ag, Co, and Ni Particles Into Thin Films at Liquid/Liquid Interfaces," *Journal of Nanoscience and Nanotechnology,* vol. 16, no. 5, pp. 5420-5425, 2016.
[13] H. Peng, Y. Liu, W. Y. Peng, J. S. Zhang, and R. Ruan, "Green Synthesis and Stability Evaluation of Ag Nanoparticles Using Bamboo Hemicellulose," *Bioresources,* vol. 11, no. 1, pp. 385-399, 2016.
[14] J. Gao, J. Xu, S. X. Wen, J. Hu, and H. L. Liu, "Plasma-assisted synthesis of Ag nanoparticles immobilized in mesoporous cellular foams and their catalytic properties for 4-nitrophenol reduction," *Microporous and Mesoporous Materials,* vol. 207, pp. 149-155, 2015.
[15] Y. H. Li, Q. Qiang, X. W. Zheng, and Z. L. Wang, "Controllable electrochemical synthesis of Ag nanoparticles in ionic liquid microemulsions," *Electrochemistry Communications,* vol. 58, pp. 41-45, 2015.
[16] A. Celebioglu, Z. Aytac, O. C. O. Umu, A. Dana, T. Tekinay, and T. Uyar, "One-step synthesis of size-tunable Ag nanoparticles incorporated in electrospun PVA/cyclodextrin nanofibers," *Carbohydrate Polymers,* vol. 99, pp. 808-816, 2014.
[17] S. Li, Q. Tao, and Q. Y. Zhang, "Transition of Growth Mode Controlled by the Density of Nuclei in Photocatalytic Synthesis of Ag Nanoparticles," *Chinese Journal of Inorganic Chemistry,* vol. 30, no. 7, pp. 1567-1574, 2014.
[18] A. I. Lukman, B. Gong, C. E. Marjo, U. Roessner, and A. T. Harris, "Facile synthesis, stabilization, and anti-bacterial performance of discrete Ag nanoparticles using Medicago sativa seed exudates," *Journal of Colloid and Interface Science,* vol. 353, no. 2, pp. 433-444, 2011.
[19] M. Grouchko, A. Kamyshny, K. Ben-Ami, and S. Magdassi, "Synthesis of copper nanoparticles catalyzed by pre-formed silver nanoparticles," *Journal of Nanoparticle Research,* vol. 11, no. 3, pp. 713-716, 2009.
[20] R. Sachan *et al.*, "Oxidation-Resistant Silver Nanostructures for Ultrastable Plasmonic Applications," *Advanced Materials,* vol. 25, no. 14, pp. 2045-2050, 2013.
[21] J. Liu *et al.*, "TAT-modified nanosilver for combating multidrug-resistant cancer," *Biomaterials,* vol. 33, no. 26, pp. 6155-6161, 2012.
[22] S. Ifuku *et al.*, "Facile preparation of silver nanoparticles immobilized on chitin nanofiber surfaces to endow antifungal activities," *Carbohydrate Polymers,* vol. 117, pp. 813-817, 2015.
[23] J. S. Kim *et al.*, "Antimicrobial effects of silver nanoparticles," *Nanomedicine-Nanotechnology Biology and Medicine,* vol. 3, no. 1, pp. 95-101, 2007.
[24] P. N. Njoki, W. J. Wu, P. Lutz, and M. M. Maye, "Growth Characteristics and Optical Properties of Core/Alloy Nanoparticles Fabricated via the Layer-by-Layer Hydrothermal Route," *Chemistry of Materials,* vol. 25, no. 15, pp. 3105-3113, 2013.
[25] A. Gillett, D. Waugh, J. Lawrence, M. Swainson, and R. Dixon, "Laser surface modification for the prevention of biofouling by infection causing Escherichia Coli," *Journal of Laser Applications,* vol. 28, no. 2, 2016, 022503.
[26] Q. Zhao and Y. Liu, "Modification of stainless steel surfaces by electroless Ni-P and small amount of PTFE to minimize bacterial adhesion," *Journal of Food Engineering,* vol. 72, no. 3, pp. 266-272, 2006.
[27] M. Ahamed, M. S. AlSalhi, and M. K. J. Siddiqui, "Silver nanoparticle applications and human health," *Clinica Chimica Acta,* vol. 411, no. 23–24, pp. 1841-1848, 2010.

[28] S. Arora, J. M. Rajwade, and K. M. Paknikar, "Nanotoxicology and in vitro studies: The need of the hour," *Toxicology and Applied Pharmacology,* vol. 258, no. 2, pp. 151-165, 2012.
[29] D. V. Sanghani, P. J. Smith, D. W. Allen, and B. F. Taylor, "A reinvestigation of some triphenylphosphine-silver halide complexes and their reaction with stannous chloride: 119mSn Mössbauer and 31P FT NMR studies," *Inorganica Chimica Acta,* vol. 59, pp. 203-206, 1982.
[30] G. L. Stansfield *et al.*, "Growth of nanocrystals and thin films at the water-oil interface," *Philosophical Transactions of the Royal Society a-Mathematical Physical and Engineering Sciences,* vol. 368, no. 1927, pp. 4313-4330, 2010.
[31] V. V. Agrawal, G. U. Kulkarni, and C. N. R. Rao, "Nature and properties of ultrathin nanocrystalline gold films formed at the organic-aqueous interface," *Journal of Physical Chemistry B,* vol. 109, no. 15, pp. 7300-7305, 2005.
[32] J. L. Hueso, V. Sebastian, A. Mayoral, L. Uson, M. Arruebo, and J. Santamaria, "Beyond gold: rediscovering tetrakis-(hydroxymethyl)-phosphonium chloride (THPC) as an effective agent for the synthesis of ultra-small noble metal nanoparticles and Pt-containing nanoalloys," *Rsc Advances,* vol. 3, no. 26, pp. 10427-10433, 2013.
[33] R. Vasudevan, A. J. Kennedy, M. Merritt, F. H. Crocker, and R. H. Baney, "Microscale patterned surfaces reduce bacterial fouling-microscopic and theoretical analysis," *Colloids and Surfaces B-Biointerfaces,* vol. 117, pp. 225-232, 2014.
[34] L. Perez, M. Flores, J. Avalos, L. S. Miguel, O. Resto, and L. Fonseca, "Comparative study of the growth curves of B-subtilis, K-pneumoniae, C xerosis and E-coli bacteria using nanometric silicon particles as a bacteriological sensor," in *Conference on Nanotechnology*, Maspalomas, Spain, 2003, vol. 5118, pp. 494-501
[35] C. Sekse, J. Bohlin, E. Skjerve, and G. E. Vegarud, "Growth comparison of several Escherichia coli strains exposed to various concentrations of lactoferrin using linear spline regression," *Microbial Informatics and Experimentation,* vol. 2, pp. 5-5, 2012.
[36] H. Fujikawa, A. Kai, and S. Morozumi, "A new logistic model for Escherichia coli growth at constant and dynamic temperatures," *Food Microbiology,* vol. 21, no. 5, pp. 501-509, 2004.
[37] J. J. Harrison *et al.*, "The use of microscopy and three-dimensional visualization to evaluate the structure of microbial biofilms cultivated in the Calgary Biofilm Device," *Biological Procedures Online,* vol. 8, pp. 194-215, 2006.
[38] J. Schindelin *et al.*, "Fiji: an open-source platform for biological-image analysis," *Nature Methods,* vol. 9, no. 7, pp. 676-682, 2012.
[39] M. P. Seah, L. S. Gilmore, and G. Beamson, "XPS: Binding energy calibration of electron spectrometers 5 - Re-evaluation of the reference energies," *Surface and Interface Analysis,* vol. 26, no. 9, pp. 642-649, 1998.
[40] "High Resolution XPS of Organic Polymers: The Scienta ESCA300 Database (Beamson, G.; Briggs, D.)," *Journal of Chemical Education,* vol. 70, no. 1, p. A25, 1993.
[41] A. V. Naumkin, A. Kraut-Vaas, S. W. Gaarenstroom, and C. J. Powell. (2012, 19-Jan). *NIST X-Ray Photoelectron Spectroscopy Database, NIST Standard Reference Database 20, v4.1*. Available: https://srdata.nst.gov/xps
[42] N. T. K. Thanh, N. Maclean, and S. Mahiddine, "Mechanisms of Nucleation and Growth of Nanoparticles in Solution," *Chemical Reviews,* vol. 114, no. 15, pp. 7610-7630, 2014.
[43] P. Asanithi, S. Chaiyakun, and P. Limsuwan, "Growth of Silver Nanoparticles by DCMagnetron Sputtering," *Journal of Nanomaterials,* 2012, 963609.
[44] K. Jyoti, M. Baunthiyal, and A. Singh, "Characterization of silver nanoparticles synthesized using Urtica dioica Linn. leaves and their synergistic effects with antibiotics," *Journal of Radiation Research and Applied Sciences,* vol. 9, no. 3, pp. 217-227, 2016.
[45] B. A. Cymes, M. P. S. Krekeler, K. N. Nicholson, and J. D. Grigsby, "A transmission electron microscopy (TEM) study of silver nanoparticles associated with mine waste from New

Caledonian nickel deposits: potential origins of silver toxicity in a World Heritage Site," *Environmental Earth Sciences,* vol. 76, no. 18, p. 640, 2017.

[46] J. L. Graves *et al.*, "Rapid evolution of silver nanoparticle resistance in Escherichia coli," *Frontiers in Genetics,* vol. 6, p. 42, 2015.

[47] M. Rai, A. Yadav, and A. Gade, "Silver nanoparticles as a new generation of antimicrobials," *Biotechnology Advances,* vol. 27, no. 1, pp. 76-83, 2009.

[48] I. Sondi and B. Salopek-Sondi, "Silver nanoparticles as antimicrobial agent: a case study on E-coli as a model for Gram-negative bacteria," *Journal of Colloid and Interface Science,* vol. 275, no. 1, pp. 177-182, 2004.

[49] Y. Jin, T. Zhang, Y. H. Samaranayake, H. H. P. Fang, H. K. Yip, and L. P. Samaranayake, "The use of new probes and stains for improved assessment of cell viability and extracellular polymeric substances in Candida albieans biofilms," *Mycopathologia,* vol. 159, no. 3, pp. 353-360, 2005.

[50] D. Perera-Costa, J. M. Bruque, M. L. González-Martín, A. C. Gómez-García, and V. Vadillo-Rodríguez, "Studying the Influence of Surface Topography on Bacterial Adhesion using Spatially Organized Microtopographic Surface Patterns," *Langmuir,* vol. 30, no. 16, pp. 4633-4641, 2014.

[51] L. V. Stebounova, E. Guio, and V. H. Grassian, "Silver nanoparticles in simulated biological media: a study of aggregation, sedimentation, and dissolution," *Journal of Nanoparticle Research,* vol. 13, no. 1, pp. 233-244, 2011.

[52] B. Reidy, A. Haase, A. Luch, K. A. Dawson, and I. Lynch, "Mechanisms of Silver Nanoparticle Release, Transformation and Toxicity: A Critical Review of Current Knowledge and Recommendations for Future Studies and Applications," *Materials,* vol. 6, no. 6, pp. 2295-2350, 2013.

[53] Y. L. Wang, Y. Z. Wan, X. H. Dong, G. X. Cheng, H. M. Tao, and T. Y. Wen, "Preparation and characterization of antibacterial viscose-based activated carbon fiber supporting silver," *Carbon,* vol. 36, no. 11, pp. 1567-1571, 1998.

[54] O. Akhavan and E. Ghaderi, "Bactericidal effects of Ag nanoparticles immobilized on surface of SiO2 thin film with high concentration," *Current Applied Physics,* vol. 9, no. 6, pp. 1381-1385, 2009.

Ref 41 last accessed: 19-1-2018